Current Optics and Photonics
Vol. 2, No. 1, February 2018, pp. 7-14

ISSN: 2508-7266(Print) / ISSN: 2508-7274(Online)
DOI: https://doi.org/10.3807/COPP.2018.2.1.007

A Novel Ramp Method Based on Improved Smoothing Algorithm and Second Recognition for Windshear Detection Using LIDAR

Meng Li[1,3]*, Jiuzhi Xu[1], Xing-long Xiong[2], Yuzhao Ma[2], and Yifei Zhao[1]

[1]*Civil Aviation Meteorological Institute, Key Laboratory of Operation Programming & Safety Technology of Air Traffic Management, Civil Aviation University of China, Tianjin 300300, China*
[2]*Tianjin Key Laboratory for Advanced Signal Processing, Civil Aviation University of China, Tianjin 30030, China*
[3]*College of Precision Instrument and Optoelectronics Engineering, Key Lab of Optoelectronic Information Technology (Ministry of Education), Tianjin University, Tianjin 300072, PR China*

(Received October 30, 2017 : revised December 13, 2017 : accepted December 14, 2017)

As a sophisticated detection technology, LIDAR has been widely employed to probe low-altitude windshear. Due to the drawbacks of the traditional ramp algorithm, the alarm accuracy of the LIDAR has not been satisfactory. Aiming at settling this matter, a novel method is proposed on the basis of improved signal smoothing and second windshear detection, which essentially acts as a combination of ramp algorithm and segmentation approach, involving the human factor as well as signal fluctuations. Experiments on the real and artificial signals verify our approach.

Keywords : LIDAR, Windshear, Signal smoothing, Second recognition
OCIS codes : (010.0280) Remote sensing and sensors, (010.3640) Lidar

I. INTRODUCTION

Known as the "the aerial killer", low-level windshear has a critical effect on aircraft flight safety, especially during the approach flight (take off and landing phase)s [1-4]. Research promoted by the International Civil Aviation Organization (ICAO) showed that in the USA windshear has represented a major contributing factor in at least 20-30 civil aviation accidents that occurred during the period from 1964 to 1985. Many different kinds of equipment have been utilized to detect and warn of the low-altitude windshear in different installation locations. Some examples include weather radar [5], airport surveillance radars [6], and numerical weather prediction [7], but LIDAR is a popular detection device that is employed to scan the wind speed and direction in a variety of ways, with the advantages of high precision and timely response [8, 9]. However, in practical applications, improvement of the alarm accuracy is a challenge [10, 11]. In 2008, a long-term statistic was performed at Hong Kong airport [11] for testing the LIDAR alarm rate, the result is only 76%, which illustrates experimentally the necessity of raising the LIDAR alarm rate.

In the past years, a series of experiments and methods have been investigated for windshear measurement. Initially, Uyeda [12] developed an algorithm that detects and tracks wind fronts automatically, which measures radial convergence and readily detects the wind propagating along radials. However, this method has not been used in practical applications. In 1993, Hermes [13] designed the ramp algorithm to detect wind fronts and to provide the recommended threshold for windshear detection. This method first addresses the operational need of the pilots in avoidance of the windshear and is regarded as a classical method in the field of civil aviation safety. In recent years, some algorithms based upon the flight condition and mathematical statistics are proposed for raising the LIDAR alarm rate. Chan [14] applied F-factor algorithm in the alerting of low-level windshear, which associates with the derivation of the total aircraft

*Corresponding author: 867750570@163.com, ORCID 0000-0003-4413-2390
Color versions of one or more of the figures in this paper are available online.

energy and its change rate. Bilgili [15] applied mean wind speeds and artificial neural networks to predict mean monthly wind speeds. Deo [16] used artificial neural networks to predict the power output of wind turbines. James applied chaotic oscillatory-based neural networks [17] to forecast the evolution of wind fields along the glide path in the vicinity of the airport with LIDAR data. But unfortunately these methods do not improve the traditional ramp algorithm, thereby having an unsatisfactory effect in the practical application. Additionally, the human individual difference is an important factor affecting the alarm rate of LIDAR. Each pilot has different experiences for estimating the windshear degree. But the F-factor method and neural networks are the enhancements of the ramp method in timely windshear detection, they do not utilize the pilots experiences in windshear detection.

In this paper, we investigate the features of the traditional ramp algorithm, and explain the issues of the ramp method from the perspectives of noise and the human factor. For overcoming these issues, we develop a novel method based upon a signal smoothing mechanism and second windshear recognition, which leads to a series of artificial simulations and actual experiments. The layout of this paper is arranged as follows. In Section 2, a brief description of the ramp algorithm is presented, and the drawbacks of this traditional method are introduced. Then the overall strategies of our method are demonstrated in the flowchart in Section 3. A systematic description is shown step-by-step. Subsequently, a series of simulations and experiments are performed to verify the proposed approach, in Sections 4 and 5. Finally, in Section.6 the conclusions are outlined.

As three mainstream methodologies of LIDAR scanning, the conventional RHI (range-height indicator) [18] and PPI (plan position indicator) [19] are mainly applied in the general overview of the winds around the airport area, while the GPS [2] (glide path scanning) can detect the wind fluctuations along the glide path, shown as Fig. 1. Therefore, The GPS has to issue the windshear alerts on a minute-to-minute basis, thereby needing a more accurate and timely windshear detection technique compared with other methods. In this paper, we propose the improved approach only applying it to the GPS.

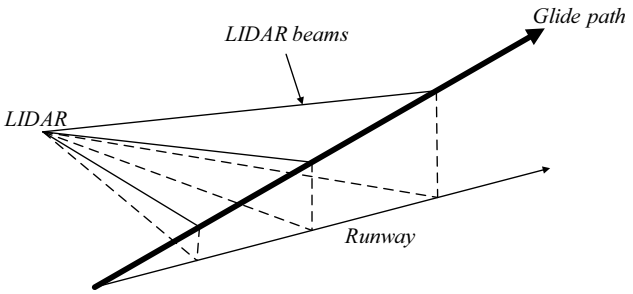

FIG. 1. Schematic diagram of glide path scan of LIDAR.

II. ORIGINAL RAMP ALGORITHM

2.1. A Brief Description of Traditional Ramp Method

The traditional ramp algorithm can be explained as an extended difference algorithm under different sampling intervals, resulting in the possible position of windshear by threshold. Signals received by LIDAR are quality controlled to remove the "spikes" arising from clutter and small-scale wind fluctuations associated with airport wake turbulence or jet exhaust. This process is completed internal to LIDAR, and retains the genuine information of the headwind. The change of headwind Δv via a distance H (ramp length) is termed as a windshear ramp, which is increased step by step, such as 400 m, 800 m, 1600 m, 3200 m, according to Ref. [20]. Aiming at alleviating the effects of velocity fluctuations and endpoints, we employ a filter to smooth the velocity increment profile, combining the lengthening method [21] with the last valid velocity data available at each end. Comparing the peaks (or troughs) in the headwind profile with the neighboring troughs (or peaks), the expansion and contraction are applied to adjust the preliminary ramp length additionally for capturing the possible full strength of the headwind change. Following the internationally alerting convention, the alert threshold could be set as 15 knots. If any one of the ramps selected by the ramp prioritization exceeds this threshold, an alert of windshear would be generated to help to pilot out of possible dangers.

For evaluating the windshear, Woodfield and Woods [22] introduced the severity factor:

$$S = \left(\frac{dV}{dt}\right)\left(\frac{\Delta V}{V_{app}}\right)^2 = \left(\frac{\Delta V}{H^{1/3}}\right)^3 \Big/ V_{app} \tag{1}$$

where ΔV is the change of headwind, $\frac{dV}{dt}$ presents the rate of wind speed change, H and V_{app} indicate the ramp length and the normal approach speed of the airplane, respectively.

2.2. The Drawbacks of the Traditional Ramp Algorithm

As a widely applied method of windshear detection in low altitude, the ramp algorithm is always limited by the alarm accuracy. Apart from uncertain factors of individual differences caused by complex interaction among aircraft, the smoothing impact as well as the human factor can also be introduced to explain these problems.

As demonstrated above, the purpose of the smoothing procedure is removing the fluctuations of the received LIDAR signals. However, the peaks and troughs carrying the useful information may be also erased unconsciously, which makes the wind changes in the processed original headwind function become indistinct, resulting in the alarm rate falling.

On the other hand, the traditional ramp method only

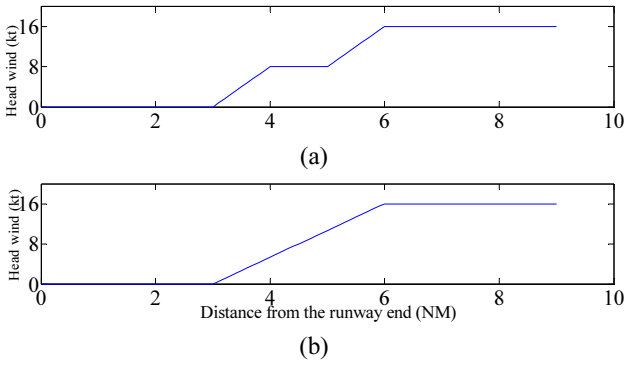

FIG. 2. The headwind profiles with common windshear (b) and special windshear that contains a flat area (a).

focuses on both end values of the single ramp, but neglects the internal features of the ramp waveform that may reflect the true feelings of the pilot. For example, in Fig. 2 can be determined as the same windshears (the wind change above 15 kt) based upon the "endpoint mechanism" of the traditional ramp approach, while in the judgment of the pilot, (a) is not considered as the windshear, for the reason that a flat curve of 4-5 km divides the entire ramp into two weak windshears below the threshold of 15 kt. In principle, due to the the pilot reports regarded as the sole criterion, the detection algorithm must be improved to adapt to the intuition of pilots.

III. A NOVEL WINDSHEAR DETECTION METHOD

Aiming at solving the above issues of the traditional ramp algorithm, we proposed a novel approach of windshear detection based on the improved signal smoothing mechanism and second windshear recognition. The flowchart and complete steps of this scheme have been shown in the following.

3.1. Weighted Smoothing Approach

After quality control and signal construction, the velocity increment profile can be obtained and termed as s_0. Smoothed by the filter, s_0 is transformed to be s_1. Bringing the unsmoothed signal s_0 and smoothed signal s_1 into the last two steps of the ramp algorithm respectively, we can obtain three possible cases shown in Table 1, which actually reveals the influence of fluctuations on the windshear determination.

For the first case, the final detected range is calculated as

$$\begin{aligned} L_1^{\,0} &= L_1 - \frac{l_1}{k+l_1}\left(L_1 - L_1'\right) \\ L_2^{\,0} &= L_2 - \frac{l_2}{k+l_2}\left(L_2 - L_2'\right) \end{aligned} \tag{2}$$

where k is the variance of the fluctuation $n = s_0 - s_1$ in $[L_1', L_2']$, l_1 and l_2 are the ones in $[L_1', L_1]$ and $[L_2, L_2']$ respectively. As shown in Fig. 3, we weight two situations of smoothing and unsmoothing, based upon the fluctuation degree acting on the ends of determined windshear.

For the second case, a judging length T_s is introduced to determine the windshear. If $L_2' - L_1' \geq T_s$, a windshear is determined; otherwise, it is not. By this scheme, the alerting system completes an integrated and comprehensive judgment.

For the third case, the windshear is obviously not determined.

TABLE 1. Three possible cases after signal processing with two kinds of "smoothing method"

	The detected windshear range for s_0	The detected windshear range for s_1
Case 1	$[L_1', L_2']$	$[L_1, L_2]$
Case 2	$[L_1', L_2']$	No windshear
Case 3	No windshear	No windshear

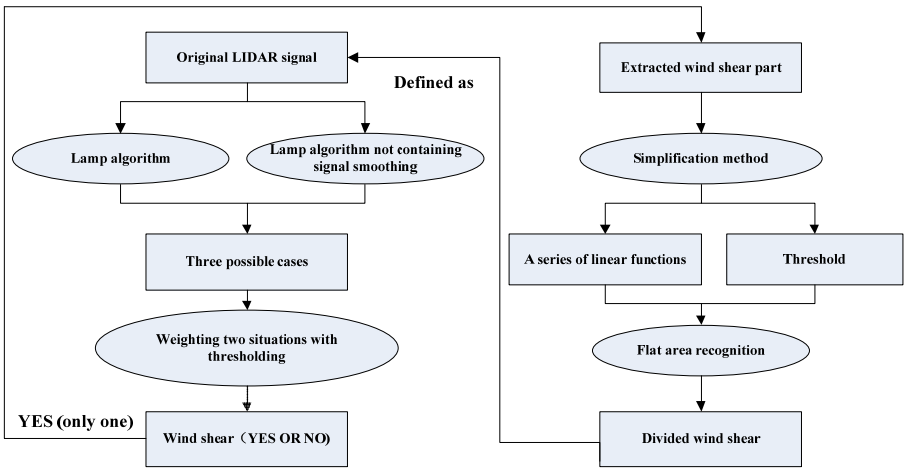

FIG. 3. The flowchart of the proposed approach for windshear detection.

3.2. The Secondary Windshear Recognition

Essentially, the key of second recognition is the flat areas detection for windshear ramp. In this procedure, we apply a simplification technique to transform the noisy headwind profile into a series of linear functions which is shown in Fig. 4. Some thresholds are set to judge the possible flat areas with the simplified signal.

1) Starting with a windshear profile s_0, extremes of s_0 are identified and termed as $(m_1, m_2, ..., m_n)$.
2) Connecting the endpoints of s_0, a linear function k_1^1 can be established.
3) Search out the extremes the furthest away from s_0, termed as m_{i_1}, and connect the m_{i_1} with the left and right endpoints. We can obtain two linear functions k_2^1 and k_2^2.
4) Regard the left endpoint and m_{i_1} as two new endpoints, and repeat the steps 2)~3). The functions k_3^1 and k_3^2 are obtained. Similarly, regarding the right endpoint and m_{i_1} as two endpoints, we can obtain k_3^3 and k_3^4.
5) Consider two neighboring searched points (containing endpoints) as the new endpoints, and bring them into step 2)~4) iteratively. We can obtain a series of end-to-end linear functions $k_n^1, k_n^2, \cdots, k_n^{2^{n-1}}$ that constitute a simplified signal, termed as s_1'.

$$s_1' = \left\{k_n^1, k_n^2, ..., k_n^{2^{n-1}}\right\} \tag{3}$$

6) Compute the derivatives of the line function $k_n^1, k_n^2, \cdots, k_n^{2^{n-1}}$, termed as $k_1, k_2, \cdots, k_n$.
7) Define a threshold T_1 to limit k_i. If $k_i < T_1$, it is considered as the flat area, otherwise, it is not. As described in Fig. 5, the flat area k_i can divide s_1 into two parts, termed as s_1^1 and s_1^2.
8) If s_1^1 and s_1^2 both are below the windshear threshold (15 kt), s_0 is not considered as the windshear.

In our method, profile simplification focuses on extracting the essential features of the headwind. By this technique, the slope characteristics of the headwind profile can be indicated clearly. However, unlike employing a two-dimensional threshold to determine a flat area, our approach combines linear simplification with a slope threshold. This design not only restrains the impact of irregular signal fluctuation through feature points extraction, but also simplifies the identification process with a series of linear functions.

IV. SIMULATIONS

As shown in Fig. 6, the three simplest headwind profiles are produced artificially, which are the common windshear, the windshear divided by a flat area as well as the one disturbed by a peak. For a simplifying algorithm, they are set to be simple linear step functions with the same wind change of 18 kt from 0.5 NM to 2 NM. In Fig. 6(b), a

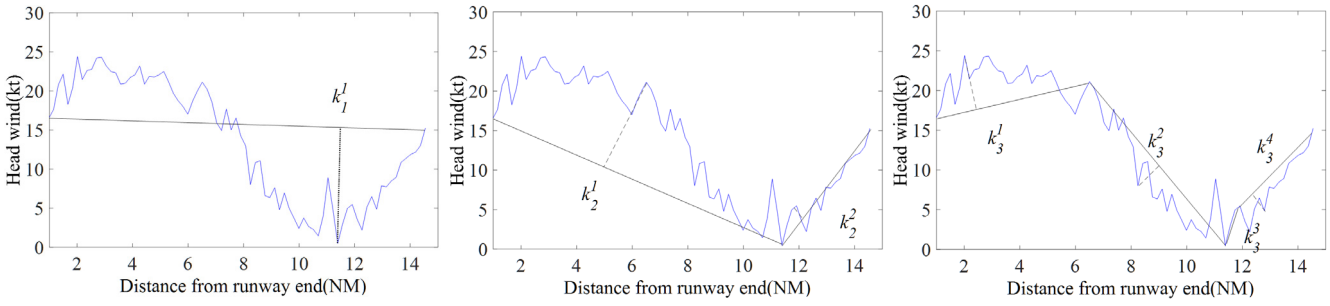

FIG. 4. Schematic diagram of simplification method: the first iteration (a), the second iteration (b) and final simplified signal (c). The curve and straight lines express the original and simplified signals, respectively.

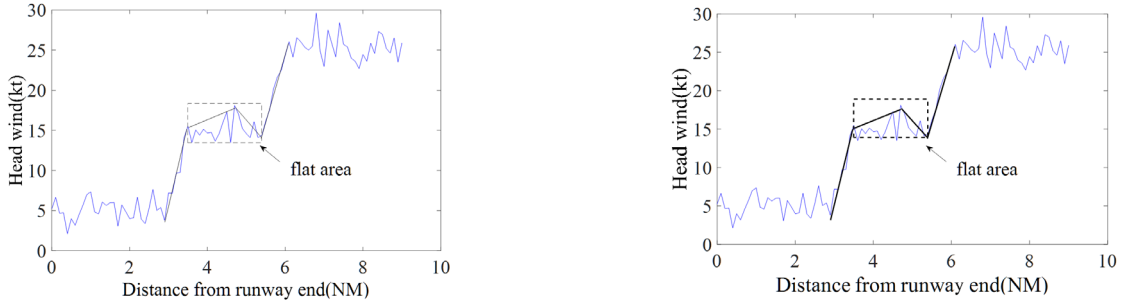

FIG. 5. Flat area detection with linear simplification method and a two-dimensional threshold.

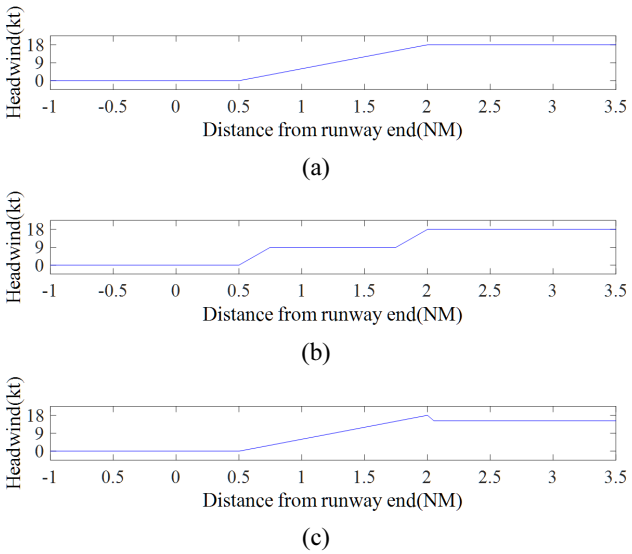

FIG. 6. Three artificial test signals: the common windshear (a), the windshear divided by a flat area (b) and one disturbed by a peak (c).

long flat line of 1.5 km divides the ramp into two parts. In Fig. 6(c), a little step of 4 kt is produced to confuse the noise interference. To test the performance of anti-fluctuation, we add Gaussian white noise into the artificial signals, resulting in three series of signals in the signal-to-noise ratio (SNR) of 15 db, 20 db and 30 db. Using the traditional ramp algorithm and our method, we process these artificial signals with $T_1 = 7.5\ kt/NM$, $T_s = 2\ NM$.

Table 2 displays the detected results using two methods. One can see the opposite results with two methods in the "flat area" and "peak" interferences, because of the slope deformation of the windshear area. However, according to the views in Section 3, the results by our method approach to the true value. In our approach, the flat areas divide the headwind into more parts, which may change the first incorrect results of windshear detection. Additionally, by the proposed smoothing method, the signal features are retained by our method. These advantages lead to more accurate windshear range. In the first column, the detection ranges (0.45-2.10 NM and 0.59-2.12 NM) approach to 0.50-2.00 NM using our method, compared with the ones (0.42-2.10 NM and 0.65-2.25 NM) using the ramp algorithm. In addition, as a classical and mature approach, the ramp algorithm is applied to combine with "flat area detection". It makes our method beneficial for practical application. As demonstrated in the first columns, the results of the two methods are almost the same and approach to the actual value in the case of high SNR (20 db and 30 db). Finally, in our view, any smoothing algorithm could erase the features of the original signal. To settle this matter, we introduce the non-smoothing signal to modify the detection results of the ramp algorithm. Reasonable results will be obtained for the disturbed signal by peak, as shown in the third column.

V. EXPERIMENT

5.1. Experiments with Pilot Reports

In Hong Kong airport, coherent Doppler LIDAR is installed for windshear detection [20], covering four runway corridors (07LA,07RA,25RA and 25LA) by GPS providing multi-angle data. By these equipment, we can obtain some timely pilot reports to test the performance of different methods.

In Fig. 7, we display two real headwind profiles at Hong Kong airport. The results of (a) and (b) are +18 kt and +16 kt far away from the pilot reports (10 kt and non-windshear) using the traditional ramp algorithm. But with our method, the original signal is divided into two parts by the flat area, thereby the windshear degree being lower and approaching to the pilot reports. Moreover, one can find that the flat area position affects the segmentation results. Obviously, half-cut has the greatest impact on secondary recognition. In addition, due to the linear function similar to "the flat area" in form, the simplified curves are beneficial for "the flat area" detection. Furthermore, from the dashed lines along the signal ramp, one can observe the signal trends are obtained completely based on the signal simplification.

5.2. Experiments with Different Waveforms

Figure 8 demonstrates four real headwind profiles involving windshears collected in Hong Kong airport at March 5 2015. The data represent four kinds of erroneous

TABLE 2. The detection results using two methods in different SNR

	The common windshear (NM)	The windshear divided by flat area (NM)	The one disturbed by peak (NM)
30 db (LA)	0.50-2.00	0.50-2.00	0.50-2.00
30 db (our method)	0.50-2.00	Non-windshear	0.50-2.00
20 db (LA)	0.42-2.10	0.60-2.11	Non-windshear
20 db (our method)	0.45-2.10	Non-windshear	0.51-1.98
15 db (LA)	0.65-2.25	0.63-2.03	Non-windshear
15 db (our method)	0.59-2.12	Non-windshear	0.69-2.09

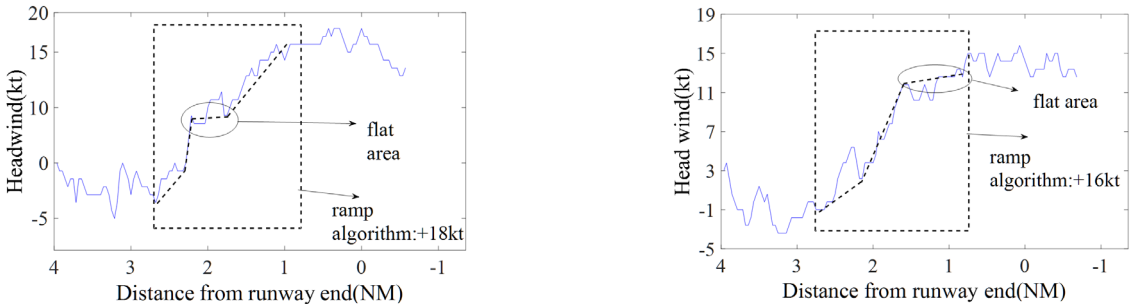

FIG. 7. Two real headwind profiles are divided by flat areas on.8:25 UTC 12 March 2007 (a) and 8:28 UTC 12 March 2007 (b). The ramp algorithm is used to determine the windshear ranges, shown as dashed boxes. Flat areas are marked by ovals. Additionally, we display the simplified curve with dashed lines. (a) Pilot report: windshear 10 kt. (b) Pilot report: non-windshear.

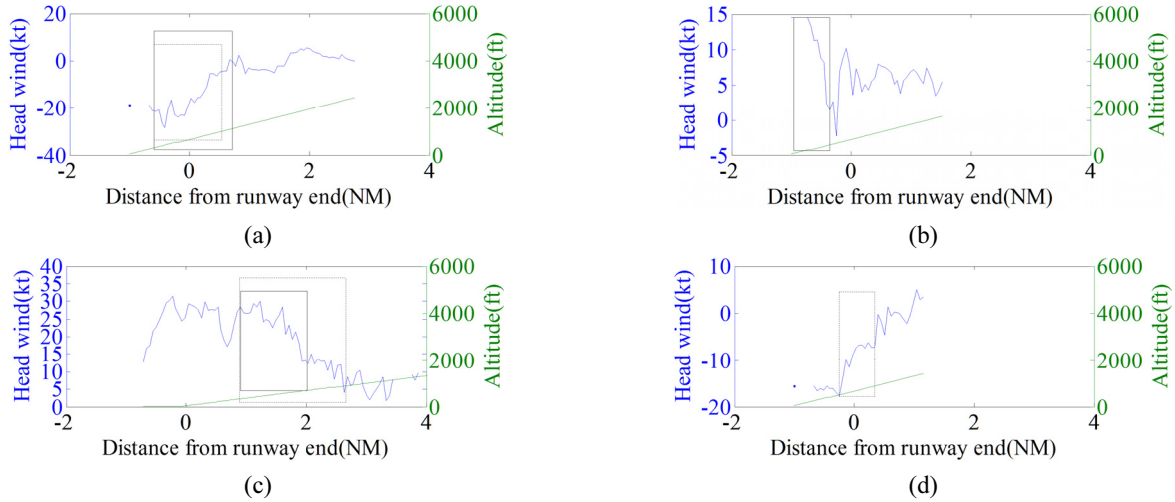

FIG. 8. The range errors of headwind profiles caused by smoothing (a) and flat area (c), and the false alarms of ones caused by smoothing (b) and flat area (d). The solid and dashed line boxes indicate the ramp algorithm and our method respectively.

determination using traditional ramp algorithm: range error caused by smoothing, alarm missing caused by smoothing, range error caused by a flat area, false alarm caused by a flat area, respectively.

In Fig. 8(a), the dash range is larger than the solid line range. However, because two neighboring spikes at the end of detection range exhibit an upward trend, and a drop appears after the highest spike, the dash range is closer to the actual situation. In addition, smoothing in the ramp algorithm obscures this rise of terminus fluctuations, thus the detection range using the ramp method is smaller than the result by our approach. In Fig. 8(b), a lowest trough is smoothed by the ramp algorithm, thereby missing the windshear. In contrast, the features of troughs are retained completely by our approach. Figs. 8(c) and 8(d) demonstrate the windshear determination with flat areas, which reveal the impact of the position and size of flat areas. In Fig. 8(c), the flat area is near the end of the detection range and cuts a small part of the windshear area, which narrows the real detection range. In Fig. 8(d), a flat area near the middle can divide the wide shear range nearly in half, thereby impacting the detection results seriously and canceling the alarms.

5.3. Long-term Comparison by Different Methods

Following the approach described in Section 3, headwind profiles along glide-paths are computed at 15 min intervals (at 00, 15, 30 and 45 min of each hour) from 2014 to 2016 over arrival corridors 25RA and 07LA of HKIA. These profiles are available at a resolution of about 100 m and cover a distance up to 6-8 km from the respective runway thresholds, depending on meteorological conditions. These alerts are validated against pilot reports of significant low-level windshear received during the study period. An event of windshear is taken as a ‘hit’ if its time of occurrence falls within 15 min interval. Performance using different methods are shown in Fig. 9. The vertical and horizontal axes are respectively the percentage of detection (PoD) and the percentage of time on alert (PoTA), defined respectively as

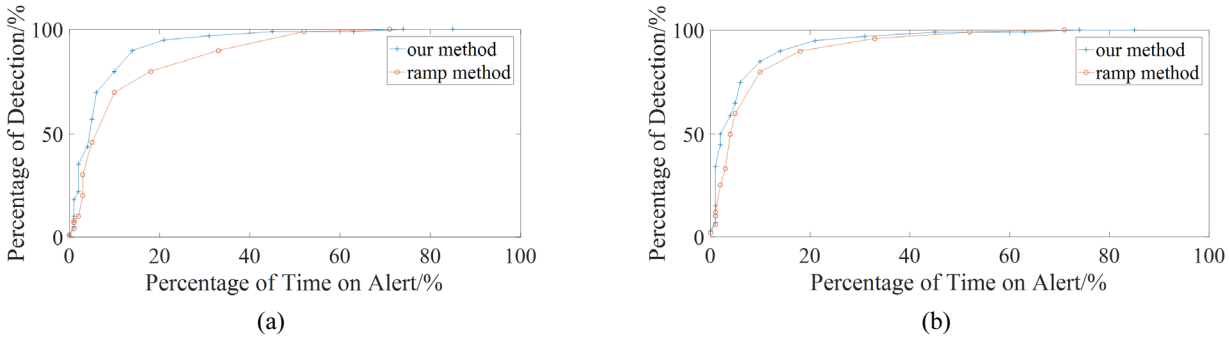

FIG. 9. The performance of low-level windshear alerting on corridors 07LA (a) and 25RA (b) at HKIA using two methods along glide-paths over January to September, 2014-2016.

$$PoD = \frac{No.of\ hits}{Total\ no.of\ pilot\ reports} \times 100\% \quad (4)$$

$$PoTA = \frac{No.of\ alerts\ issued}{Total\ no.of\ 15\,\min\ interval} \times 100\% \quad (5)$$

It can be readily observed that the headwind -based alerts by our approach show considerable skill with PoD around 80% at PoTA of 10% for both corridors. Moreover, a slight gain in PoD can be obtained by issuing alerts using our method (4-10% for 07LA, 2-5% for 25RA), for comparison with the traditional ramp method. The operational LIDAR-based windshear alerting for windshear detection algorithm based upon improved smoothing algorithm and second recognition, was able to capture 80.6% (78.9%) of pilot reports at an alert duration of 10%.

VI. CONCLUSION

In this paper, we propose a synthesized scheme of windshear detection. Smoothing impact as well as second windshear detection are creatively used to improve the traditional ramp algorithm. By the range correction and flat area detection, the original signal is simplified and divided into more parts. This process modifies the windshear range and strength, which leads to a new determination of windshear depending on the pilot‘s instincts. Artificial simulations and real signal experiments are performed to verify the framework of the proposed method effectively. However, as free and important parameters, the thresholds affect the hit and false alarm rate directly. It will be considered as the most important direction for research in the future.

ACKNOWLEDGMENT

Thanks to “The National Natural Science Foundation of China (U1433202 and U1533113)” and “The Fundamental Research Funds for the Central Universities (CAUC-3122 016D027)” for supporting this work.

REFERENCES

1. C. Moscardini, F. Berizzi, M. Martorella, and A. Capria, “Signal spectral modelling for airborne radar in the presence of windshear phenomena,” IET Radar Sonar Navigation **5**(7), 796-805 (2011).
2. K. K. Hon and P. W. Chan, “Application of LIDAR -derived eddy dissipation rate profiles in low -level wind shear and turbulence alerts at Hongkong international airport,” Meteorol. Appl. **21**(1), 74-85 (2014).
3. M. J. Ma, C. Lin, S. R. Zhao, B. K. Zhang, H. X. Shen, S. G. Wang, “Characteristics and a numerical study of low-level windshear over Beijing Capital International Airport,” J. Lanchow Univ., Nat. Sci. **7**(49), 354-360 (2013).
4. R. B. Wu, Z .C. Meng, Y. Fan, Z. G. Sun, X. G. Lu, and J. H. Huang, “Windshear signal simulation of the airborne weather radar,” Modern Radar **8**(34), 74-78 (2012).
5. J. Gao and Y. Zhao, “Simulation research on windshear prediction of airborne weather radar,” *Virtual Reality and Visualization* (ICVRV), 2014 International Conference on. **8**, 435-438 (2014).
6. M. E. Weber and M. L. Stone, “Low altitude windshear detection using airport surveillance radars,” IEEE Aerosp. Electron. Syst. Mag. **10**(6), 3-9 (1995).
7. N. Chen, Z. Qian, and X. F. Meng, “Wind power forecasts using gaussian processes and numerical weather prediction,” IEEE Trans. Power Syst. **29**(2), 656-665 (2014).
8. S. C. Medeiros, S. C. Hagen, and J. F. Weishampel, “A random forest model based on LIDAR and field measurements for parameterizing surface roughness in coastal modeling,” IEEE J. Sel. Topics Appl. Earth Observ. Remote Sens. **8**(4), 1582-1590 (2015).
9. M. Wang and Y. H. Tseng, “Automatic segmentation of LIDAR data into coplanar point clusters using an octree-based split-and-merge algorithm,” Photogramm. Eng. Remote Sens. **76**, 407-420 (2010).
10. K. K. Hon and P. W. Chan, “Application of LIDAR-derived eddy dissipation rate profiles in low-level windshear and turbulence alerts at Hong Kong international airport,” Meteorol. Appl. **21**, 74-85 (2014).
11. C. M. Shun and P. W. Chan, “Applications of an infrared doppler LIDAR in detection of windshear,” J. Atmos. Oceanic Technol. **5**(25), 637-655 (2008).
12. H. Uyeda and D. S. Zrnic, “Automatic detection of gust

fronts," J. Atmos. Oceanic Technol. **3**(1), 36-50 (1986).
13. L. G. Hermes, A. Witt, S. D. Smith, D. Klingle-Wilson, D. Morris, G. J. Stumpf, and M. D. Eilts, "The gust-front detection and wind-shift algorithms for the terminal doppler weather radar system," J. Atmos. Oceanic Technol. **10**(5), 693-709 (1993).
14. Y. F. Lee and P. W. Chan, "LIDAR-based F-factor for wind shear alerting: different smoothing algorithms and application to departing flights," Meteorol. Appl. **21**(1), 86-93 (2014).
15. M. Bilgili, B. Sahin, and A. Yasar, "Application of artificial neural networks for the wind speed prediction of target station using reference stations data," Renewable Energy **32**(14), 2350-2360 (2007).
16. A. More and M. C. Deo, "Forecasting wind with neural network," Mar. Struct. **16**(1), 35-49 (2003).
17. N. K. Liu, K. M. Kwong, and P. W. Chan, "Chaotic Oscillatory-based neural network for windshear and turbulence forecast with lidar data," IEEE Trans. Syst., Man, Cybern., Part C **10**(6), 1412-1423 (2012).
18. K. Nakamura, K. Muramoto, and T. Ohigashi, *Visualization of water vapor distribution in the lower atmosphere using two LIDARs* (ICROS-SICE International Joint Conference 2009), pp. 5445-5450.
19. N. Manago and G. Bagtasa, *Multi-wavelength LIDAR system for the characterization of tropospheric aerosols and clouds* (2012 IEEE International Geoscience and Remote Sensing Symposium), pp. 2505-2508.
20. P. W. Chan, C. M. Shun, and K. C. Wu, *Operational LIDAR-based system for automatic windshear alerting at the Hong Kong international airport* (12th Conference on Aviation, Range, and Aerospace Meteorology, 2006).
21. J. Lihui, Y. Yan, X. Xinglong, C. Bowei, C. Xing, and Z. Dian, "Doppler LIDAR alerting algorithm of low-level windshear based on ramps detection," Infrared Laser Eng. **45**(1), 106001-0106001 (2016).
22. A. A. Woodfield and J. F. Woods. *Worldwide experience of windshear during 1981-1982* (AGARD Flight Mechanics Panel Conference on 'Flight Mechanics and System Design Lessons from Operational Experience', 1983).